

Hybrid scintillators for x-ray imaging

Clifford Bueno, Richard L. Rairden, and Robert A. Betz

Lockheed Martin Missiles & Space  
Advanced Technology Center  
O/93-60, B/203, 3251 Hanover Street  
Palo Alto, CA 94304  
(415) 354-5270

**ABSTRACT**

The objective of this effort is to improve x-ray absorption and light production while maintaining high spatial resolution in x-ray imaging phosphor screens. Our current target is to improve screen absorption efficiency and screen brightness by factors of 2 or greater over existing screens that have 10-lp/mm resolution. In this program, commercial phosphor screens are combined with highly absorbing, high-resolution scintillating fiber-optic (SFO) face plates to provide a hybrid sensor that exhibits superior spatial resolution, x-ray absorption, and brightness values over the phosphor material alone. These characteristics of hybrid scintillators can be adjusted to meet specific x-ray imaging requirements over a wide range of x-ray energy. This paper discusses the design, fabrication, and testing of a new series of hybrid scintillators.

Keywords: phosphors, x-ray, luminescent devices, fiber optics, scintillators, hybrid, glass, luminescent glass, x-ray detectors

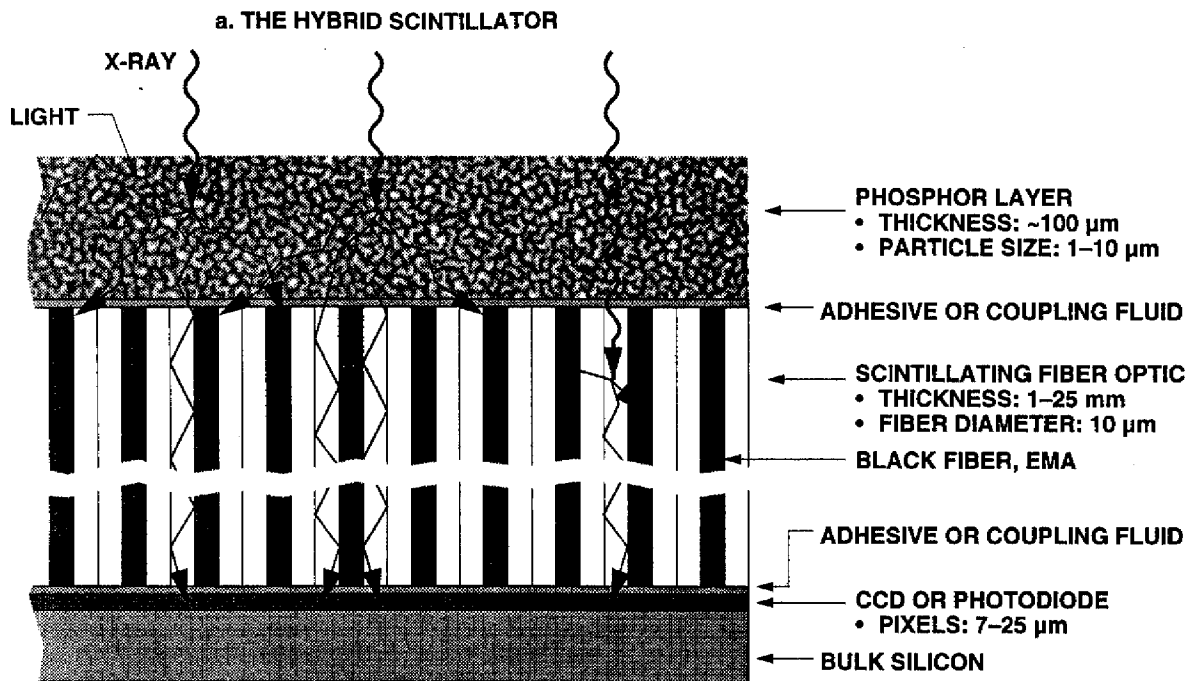
**1. INTRODUCTION**

The hybrid scintillator (or hybrid luminescent device) consists of a phosphor layer coupled to a scintillating fiber-optic (SFO) face plate. Figure 1 provides a schematic cross section of the device. The SFO is composed of an array of millions of luminescent fibers, with each fiber surrounded by a cladding glass. The fibers produce light in proportion to the x-ray intensity absorbed. The SFO also collects light from the radiation-induced emission in the overlying phosphor. Light photons produced within each fiber and in the phosphor layer are captured within fibers and are guided to the exit face of the SFO. This produces an image plane corresponding to the various intensities of light produced by the absorbed penetrating radiation. The hybrid plate can be placed in direct contact with a film or electronic sensor, such as a charge-coupled device (CCD), photodiode, or photocathode, for image visualization, or a camera utilizing a lens or fiber optics can be used to capture the image. Black fibers, also known as extramural absorption (EMA) fibers, are placed into the SFO face plate, in a ratio of as few as one for every six to eight scintillating fibers, to absorb stray, nonguided light in the face plate.

A number of optical advantages result from the use of a fiber-optic intermediary stage between the phosphor and the sensor. Figure 2 shows the problem of phosphor stray light capture by a pixelized sensor. The sensors used in today's electronic radiographic systems are typically composed of a CCD, a photodiode (such as a linear array or an amorphous silicon area array), or a photocathode (such as configured in an x-ray image intensifier system). This figure also shows that the sensor and its associated electronics, either aft or adjacent to the sensor, are exposed to radiation that can damage the device or possibly add noise to the imagery produced. Noise can be produced because some sensors and associated electronics produce large local, random (noncorrectable) signals from absorbed x-ray photons.

The use of a thick fiber-optic device between the phosphor layer and the electronic sensor offers the potential for x-ray shielding and light collimation, yielding low-noise, high-quality imagery. The use of a fiber-optic component with a low numerical aperture (NA), i.e., 0.6 or less, restricts the light acceptance and exitance angles and preserves the spatial information in the image. By making the fiber-optic stage a scintillating fiber-optic face plate, the added x-ray absorption is converted into light to provide further sensitivity.

One potential drawback with the use of a thick x-ray sensor is that it is sensitive to contrast degradation through x-ray crosstalk within the material. X-ray crosstalk arises from a divergent x-ray beam through the material. For the standard SFO face plate, as the x-ray energy increases, the x-ray cone beam (or fan beam) penetrates further into the plate, resulting in a decrease in the low-frequency modulation transfer function (MTF), i.e., the long-range spatial resolution. In general, this x-ray crosstalk does not preclude detecting features in the high spatial frequency regime. This parallax effect worsens as the x-ray



- SFO WITH NUMERICAL APERTURE OF 0.6 RESTRICTS ENTRANCE ANGLE OF PHOSPHOR LIGHT AND EXIT ANGLE OF SFO LIGHT
- SFO ENHANCES X-RAY CAPTURE/CONVERSION
- SFO SHIELDS CCD/PHOTODIODES
- THICK SFO PLATES REDUCE OPTICAL CROSSTALK

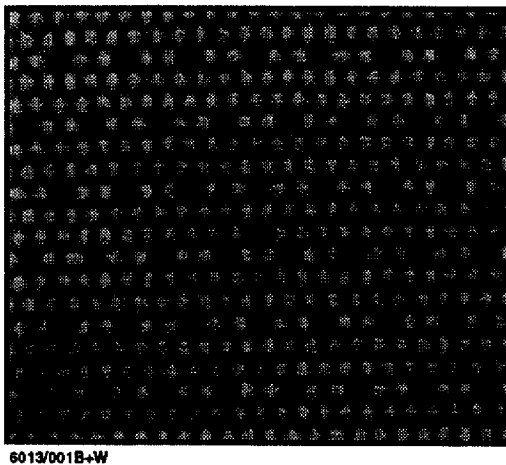


Fig. 1. (a). Cross-section schematic of the hybrid scintillator with a black EMA fiber every third fiber. (b) Photomicrograph of the SFO portion of the hybrid scintillator showing the same EMA loading, every third fiber and every third row.

penetration depth into the material increases. Luminescent materials, such as fibers of CsI, and thicker particulate phosphor materials are also prone to crosstalk degradation. However, unlike these materials, the glass SFO face plate can be configured to reduce x-ray crosstalk by glass “slumping” techniques,<sup>1</sup> in which the glass is slumped around its central axis to arrange the fibers to be collinear with the impinging cone beam. The slightly curved surface that results (curve facing away from the

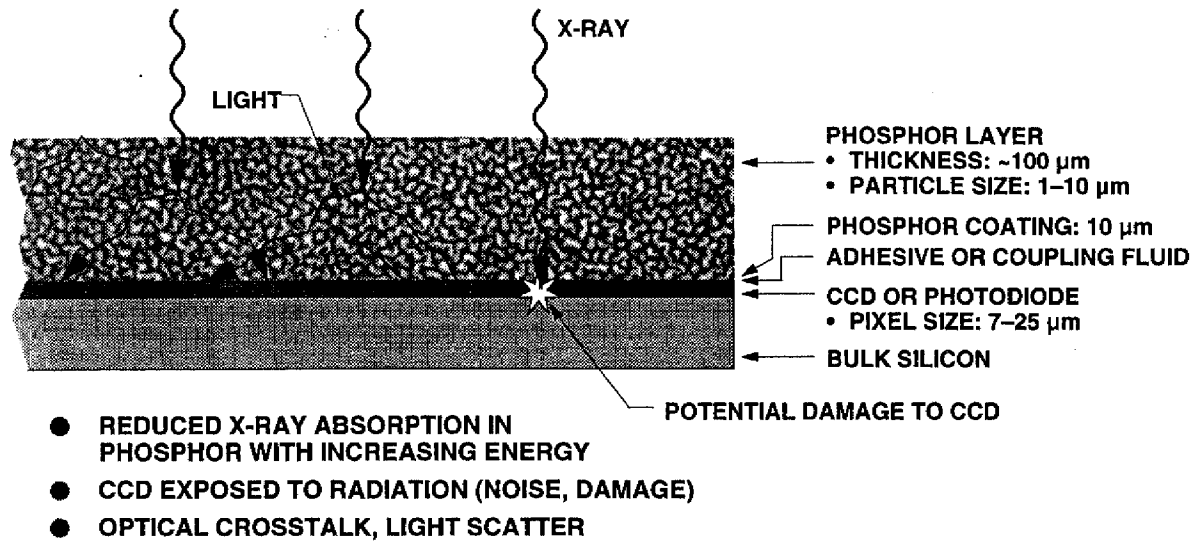


Fig. 2. Cross-section schematic of a phosphor layer over a pixelized sensor.

camera), can be used as is, i.e., with a lens, or can be machined flat for direct contact onto the input of the electronic sensor. In many low-x-ray-energy applications (<60 kV), excellent image quality can be obtained from thick SFO plates, without special treatment.

Making the SFO face plates thin to limit the x-ray penetration depth also reduces x-ray crosstalk. However, the x-ray absorption efficiency is not as high, and brightness gains are reduced. The results in this paper demonstrate that even with the potential reduction in low-frequency MTF associated with thick face plates, the overall spatial resolution of the SFO remains higher than that of high-spatial-resolution phosphor screen materials commonly used today. In most cases, the optical filtering and light collimating effects of the SFO outweigh the degrading effects of x-ray crosstalk and result in enhanced image quality. By combining the SFO and a phosphor, the effects of crosstalk are somewhat diminished by the signals produced by the thin phosphor screen. The guided light from long (as long as 19-mm) 10- $\mu\text{m}$  fibers in the SFO of the hybrid, in turn, contributes increased sharpness to the image, while enhancing x-ray capture and conversion.

Therefore, the use of an phosphor/SFO/sensor combination results in the following improvements over a phosphor/sensor configuration alone:

- Improved signal-to-noise ratio (SNR) levels through enhanced x-ray capture and conversion
- Enhanced spatial resolution through light collimation and stray-light rejection
- Lowered radiation damage to electronic sensors and reduced radiation-induced noise levels

Note that these improvements are obtained with the hybrid scintillator either in direct, intimate contact with a sensor, or through capture by a lens or fiber-optic image transfer element.

## 2. DESIGN AND FABRICATION OF THE HYBRID SCINTILLATOR

The phosphor layer in the hybrid scintillator may be selected from any of a host of x-ray phosphor materials to couple to the SFO, such as  $\text{Gd}_2\text{O}_2\text{S:Tb}$  or  $(\text{ZnCd})\text{S:Ag,Cu}$ . The physical and chemical properties of the phosphor layer, the SFO, and the interfacial region can be adjusted to obtain the desired characteristics in spatial resolution and combined brightness of the final device. A low-afterglow inorganic luminescent glass material that is activated with  $\text{Tb}^{3+}$  yields an effective SFO face plate for use in the device.<sup>2</sup> The selection and fabrication of the constituents of the hybrid scintillators tested in this study are described in the subsections below.

### 2.1. SFO selection

A number of new scintillating glass materials have been designed, prepared and tested in this laboratory for potential use as x-ray imaging sensors.<sup>2-6</sup> These materials were compared to luminescent glass materials and inorganic phosphor screens avail-

able elsewhere, in terms of x-ray attenuation, material density, x-ray-to-light conversion efficiency, emission wavelength, luminescent decay characteristics, and afterglow. A Lockheed Martin Missiles & Space (LMMS) luminescent glass material designated LKH-6 was selected for use in this study based on comparisons published previously.<sup>6</sup> Collimated Holes, Inc. (CHI), Campbell, CA, produced the SFO face plates, using the LKH-6 material as the core glass. First, the glass was cast into rods, which were fitted into glass sleeves, the cladding. These were then drawn into single hexagonal fibers, with the surrounding cladding glass essentially fused to the core fiber. These were cut and packed into hexagonal multifiber bundles, which were then drawn a second time. A set of black fibers (EMA) was prepared similarly and mixed in set positions in the bundles before this re-draw. The re-drawn multifiber bundles were sized, stacked, and fused together. The fiber-optic boule produced (~4 in. long) was then cut, ground, and polished into ~ 2 x 2 in. square face plates of different thicknesses. Table 1 lists the properties of the core glass material<sup>6</sup> of the face plate, and the corresponding fiber-optic properties used in the experiments in this paper.

Table 1. Properties of the LKH-6 SFO used in this study.

Density, core glass (g/cm <sup>3</sup> )	3.5
Density, fiber-optic face plate (g/cm <sup>3</sup> )	3.3
Effective atomic number, core glass (z)	31
n <sub>d</sub> core	1.59
n <sub>d</sub> cladding	1.47
Numerical Aperture (NA)	0.6
Fiber size (μm)	10
Thickness (in.)	0.06–0.5
Peak emission wavelength (nm)	545
Luminescent decay to 40% intensity (ms)	2.1

Although the density and atomic number give rise to a smaller x-ray attenuation than typically used x-ray phosphor screens, the use of thick glass provides substantial improvements in x-ray absorption efficiency.<sup>6</sup> Plates of different thickness were used in this study. For comparison purposes, a metallic mirror film was used on the x-ray input surface of some of the SFO plates without phosphor coatings. The mirror increases the light levels by a factor of approximately 1.8 over the SFO without the mirror, since collimated light that would have been lost is reflected back toward the CCD. Figure 3 lists the SFO specifications and thicknesses used in each experiment.

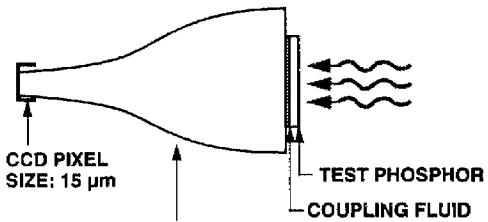
## 2.2. Phosphor selection

A commercial x-ray phosphor screen was used as part of the hybrid assembly. A high resolution Kodak Lanex Fine phosphor screen (Gd<sub>2</sub>O<sub>2</sub>S:Tb, 50 mg/cm<sup>2</sup>) was acquired and tested in a number of configurations. In each case, the phosphor was temporarily adhered to the fiber-optic component using Dow Corning Q2-3067 optical grease. The use of the optical coupling grease at these interfaces improves spatial resolution by a factor of approximately 20 to 30%; however, brightness levels decreased by an equivalent amount. Figure 3 provides the coupling schemes for the Lanex Fine phosphor screen in the experiments performed.

## 2.3. Nonscintillating fiber-optic face plates

Nonscintillating fiber-optic (NSFO) input windows are frequently used to couple phosphors to CCDs. In this paper, the resolution and brightness levels of the SFO and NSFO face-plate phosphor/CCD coupling schemes are compared. NSFO face plates of 0.6 and 1.0 NA, acquired from CHI, were used as controls in these studies. Comparative NSFO and SFO phosphor coupling tests were carried out under identical experimental conditions. The properties of the NSFO face plates are listed in Table 2. Figure 3 provides the coupling schemes used for these NSFO face plates.

a. EXPERIMENT #1

CAMERA CONFIGURATION	TEST SAMPLES	TESTING
 <ul style="list-style-type: none"> <li>● FIBER-OPTIC TAPER</li> <li>● N A: 1.0 AT OUTPUT, 0.3 AT INPUT</li> <li>● FIBER DIAMETER: 10 μm INPUT, 3 μm OUTPUT</li> <li>● EMA</li> <li>● DEMAG. = 3.3:1 RATIO</li> </ul>	<p><b>LKH-6 SFO</b></p> <ul style="list-style-type: none"> <li>● 12 mm THICK</li> <li>● MIRROR BACKING</li> <li>● 10-μm FIBERS</li> <li>● EMA FIBERS EVERY 5 FIBERS, EVERY FIVE ROWS</li> <li>● COUPLING GREASE</li> </ul> <p><b>LANEX FINE PHOSPHOR</b></p> <ul style="list-style-type: none"> <li>● 50 mg/cm<sup>2</sup> Gd<sub>2</sub>O<sub>2</sub>S:Tb</li> <li>● 100 μm THICK</li> <li>● COUPLING GREASE</li> </ul> <p><b>LKH-6 SFO/LANEX FINE</b></p> <ul style="list-style-type: none"> <li>● COUPLING GREASE AT ALL INTERFACES</li> </ul>	<ul style="list-style-type: none"> <li>● MTF AT 40, 80, AND 120 kV</li> <li>● BRIGHTNESS LEVELS IN DIGITAL COUNTS ON THE CCD OFF THE EDGE IN ABOVE MEASUREMENTS</li> </ul>

b. EXPERIMENT #2

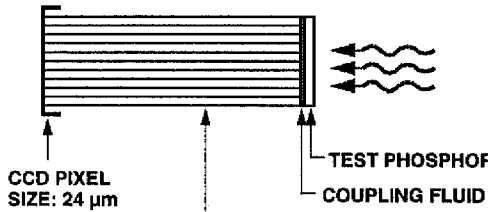
CAMERA CONFIGURATION	TEST SAMPLES	TESTING
 <ul style="list-style-type: none"> <li>● FIBER-OPTIC CONDUIT</li> <li>● N. A.: 1.0</li> <li>● FIBER DIAMETER: 6 μm</li> <li>● EMA</li> </ul>	<p><b>LKH-6 SFO</b></p> <ul style="list-style-type: none"> <li>● 2 mm THICK</li> <li>● 12 mm THICK</li> <li>● BOTH MIRROR-BACKED</li> <li>● 10-μm FIBER</li> <li>● EMA EVERY 5 FIBERS EVERY 5 ROWS</li> <li>● COUPLING GREASE</li> </ul> <p><b>LANEX FINE PHOSPHOR</b></p> <ul style="list-style-type: none"> <li>● WITH AND WITHOUT COUPLING GREASE</li> </ul>	<ul style="list-style-type: none"> <li>● MTF AT 50 kV</li> <li>● RELATIVE EXPOSURE LEVELS REQUIRED TO REACH 2400 DIGITAL COUNTS AT CCD IN SAME MTF MEASUREMENT (RELATIVE BRIGHTNESS)</li> </ul>

Fig. 3. Camera configurations and phosphor coupling schemes employed in this study. (1 of 2)

3. Camera Test Systems

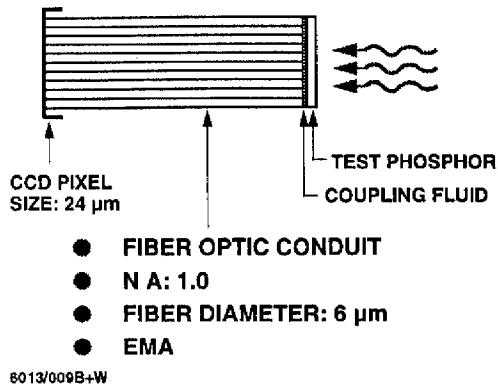
Two low-noise CCD camera systems built to LMMS specifications by Advanced Technologies, Tucson, AZ, were used to test the hybrid scintillators. Figure 3 provides schematics of the camera configurations.

3.1. Camera configuration #1

This camera consists of a 3.3:1 fiber-optic image reducer. The fiber-optic image reducer (also known as a taper) has an effective NA of 0.3 (1.0/3.3). The reducer transfers a 2 x 2 in. image to a Loral 1024 x 1024, 3-phase, full-frame CCD composed of 15-μm pixels. The CCD is cooled by a thermoelectric cooler to -35°C. The camera system used is a very low noise system with a dynamic range of approximately 4000:1. The Nyquist frequency of the camera system is 10 lp/mm at the input to the taper. Details of the camera system were reported previously.<sup>7,8</sup> Figure 3a provides a schematic of the camera system used for experiment #1 (see Section 4.1).

c. EXPERIMENT #3

**CAMERA CONFIGURATION**



**TEST SAMPLE**

**LANEX FINE ON LKH-6 SFO**

- SFO 7 mm THICK
- 10- $\mu$ m FIBERS
- EMA EVERY 5 FIBERS EVERY 5 ROWS
- COUPLING GREASE

**LANEX FINE ON 0.6 NA NSFO**

- SFO 5 mm THICK
- 6- $\mu$ m FIBERS
- NO EMA
- COUPLING GREASE

**LANEX FINE ON 1.0 NA NSFO**

- SFO 5 mm THICK
- 6- $\mu$ m FIBERS
- NO EMA
- ALL INTERFACES WITH COUPLING GREASE

**TESTING**

- SPATIAL RESOLUTION BY OBSERVATION OF LINE PAIR GAUGE AT 70 kV
- BRIGHTNESS LEVELS MEASURED AT 70 kV, 120 kV, AND 160 kV RELATIVE TO LANEX FINE/0.6 NA NSFO

Fig. 3. Camera configurations and phosphor coupling schemes employed in this study. (2 of 2)

Table 2. Properties of the NSFO face plates used in this study.

Properties of CHI face plates	NSFO#1	NSFO#2
Numerical Aperture (NA)	0.6	1.0
Fiber size ( $\mu$ m)	6	6
Thickness (in.)	0.2	0.2
Diameter (in.)	1.6	1.6
EMA	No	No

**3.2. Camera configuration #2**

This camera uses a 2048 x 2048 SITe CCD with 24- $\mu$ m pixels, which has a fiber-optic conduit input window with a magnification of unity. This results in an array size of 2 x 2 in., equivalent to camera configuration #1, but with double the resolution, 20 lp/mm. A number of applications in aerospace x-ray imaging require close to this spatial resolution. A nonreducing fiber-optic conduit was attached to this CCD to facilitate high-resolution imaging and testing of different phosphor configurations. The fiber-optic conduit is 4 in. long, contains EMA, and has 6- $\mu$ m-diameter fibers. The numerical aperture of the conduit is 1.0. These characteristics were selected so that the phosphor screen (plate) coupling to the input of the conduit would simulate direct input to the CCD. Physical coupling directly to a CCD is possible, but repeated attachments and extractions of phosphors (especially with coupling grease) would damage the electronic device. This configuration is similar to coupling schemes where the phosphor is in intimate contact with an amorphous silicon array or small CCD sensors. Details of this camera system were published previously.<sup>8,9</sup> Figure 3b and Fig. 3c provide schematics of the camera configurations used in experiments #2 and #3 (see Sections, 4.2 and 4.3).

#### 4. Measurements

Figure 3 provides schematics of the experiments reported in this paper. Details on the phosphors, fiber-optic elements and camera systems were discussed in sections 2 and 3.

##### 4.1. Experiment #1, input into a fiber-optic taper/CCD, the 10-lp/mm camera

Figure 3a provides a summary of experiment #1. A Loral 1024 CCD with an attached fiber-optic taper input window was used for imaging. The phosphors/plates were attached to the input of the taper by Dow Corning Q2-3067 coupling grease, which was also used to attach the Lanex Fine phosphor to the SFO. Spatial resolution and brightness were measured quantitatively and qualitatively on the three phosphors at 40, 80, and 120 kV. Figures 4 through 6 provide modulation transfer function data comparing the spatial resolution of each screen at these three energies. See the appendix (Section 9) for details of this measurement. Figure 7 charts the CCD signal levels measured from bypass levels taken outside the tungsten edge in these studies. The CCD pixel size is  $50\ \mu\text{m}$  (10 lp/mm) for this camera and is the limiting factor in spatial resolution in these measurements. The MTF measurements made illustrate the effect that different high-resolution phosphors have as a function of spatial frequency on this x-ray imaging system.

The x-ray source used was a Kevex 160-kV microfocus x-ray unit. The focal spot size was 0.25 mm. This focal spot provided 1.02 mA at 40 and 80 kV and 0.66 mA at 120 kV. Beam filtration was added at the source to simulate the beam hardness experienced in practice: 0.125 in. of pure aluminum at 40 kV and 0.25 in. of pure aluminum at 80 and 120 kV. The source-to-screen distance was 36.5 in. A thin tungsten edge was used at an angle to the CCD pixel array to acquire MTF results. All edge pictures were normalized for gain and offset under the same x-ray parameters, but with the edge removed. This flattens the nonuniformities and fixed patterns in the image and shifts the bias/dark levels to zero. In addition to reproducible MTF measurements, this allows quantitative brightness measurements from the same image file.

##### 4.2 Experiment #2, input into a fiber-optic conduit/CCD, the 20-lp/mm camera

Experiment #2 used a SITe 2048 x 2048 CCD with a nonreducing fiber-optic conduit input window. Figure 3b provides a summary of this experiment. Unlike the 10-lp/mm ( $50\text{-}\mu\text{m}$  pixel) camera, the CCD pixel size of  $24\ \mu\text{m}$  (20 lp/mm) in this camera is less important in limiting the overall spatial resolution of the system. An initial experiment was performed with this 20-lp/mm camera to determine the baseline spatial resolution of the LKH6-SFO and the Lanex Fine phosphor, each separately attached directly to the input of the fiber-optic conduit. MTF and light measurements were made on 12- and 2-mm-thick mirror-backed SFOs and a Kodak Lanex Fine screen attached directly to the conduit. The Lanex Fine was measured twice, once with optical coupling fluid and once with just physical contact across an air interface. The tests were made under 50-kV

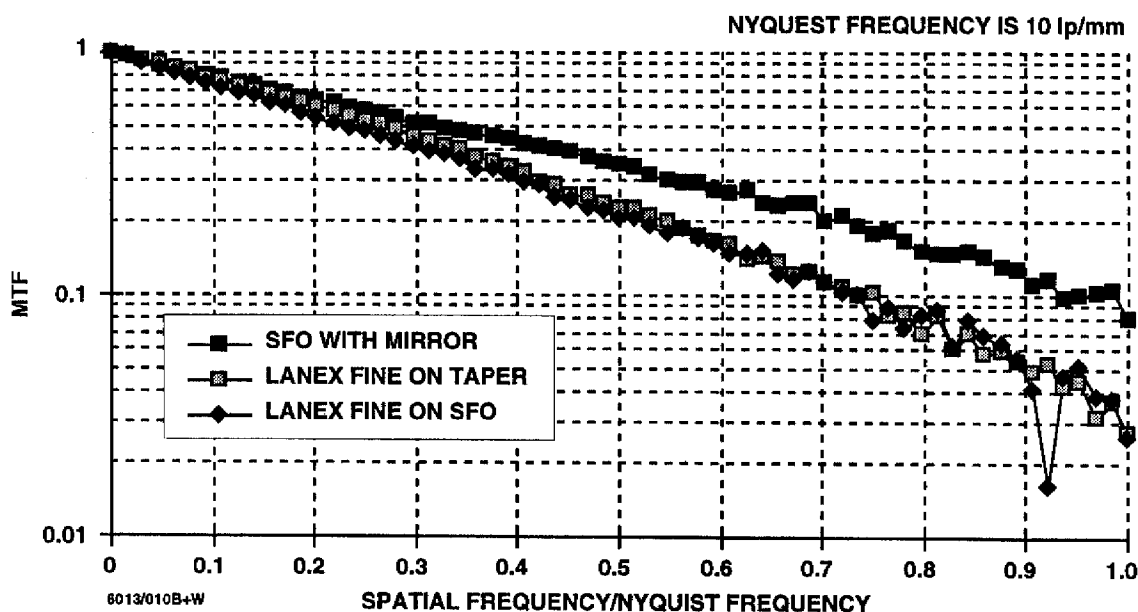


Fig. 4. MTF measurements at 40 kV.

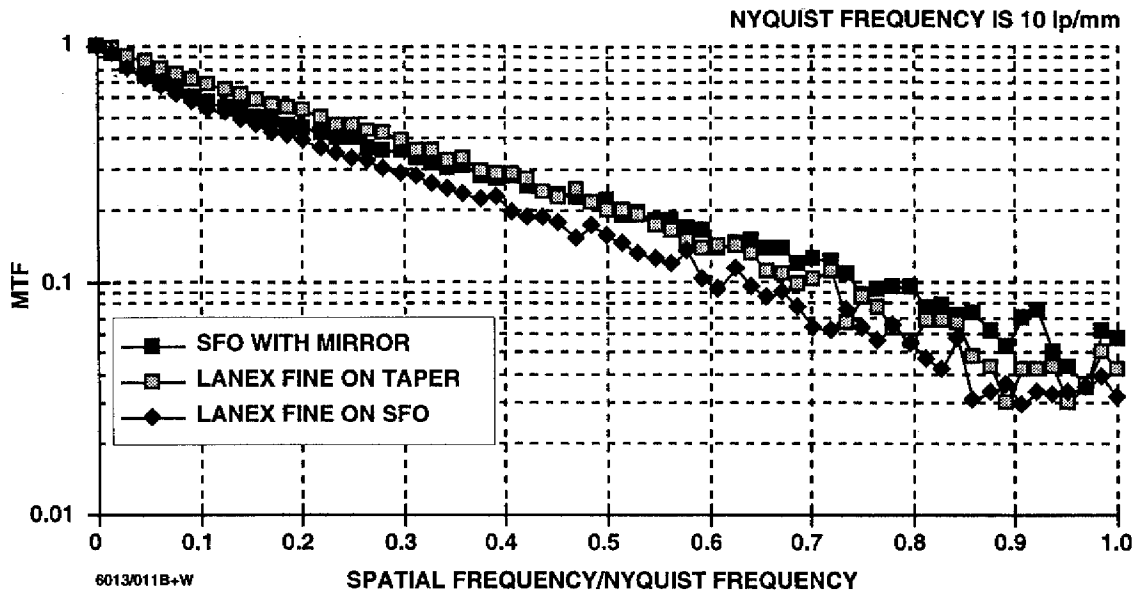


Fig. 5. MTF measurements at 80 kV.

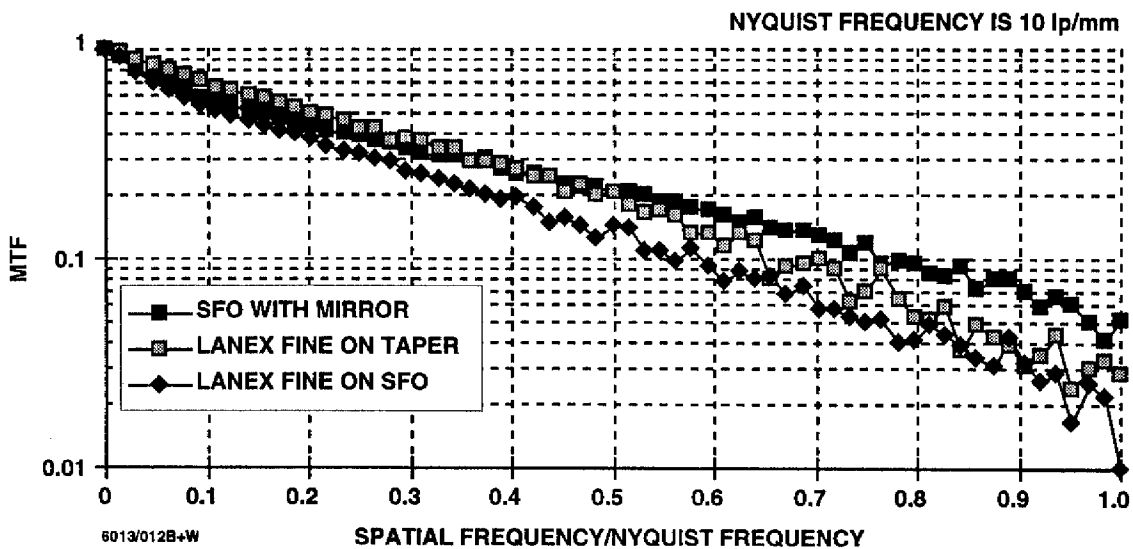


Fig. 6. MTF measurements at 120 kV.

x-rays using a Kevex 160 microfocus unit. The large focal spot, 0.25 mm, was used, and no additional filtration was employed. In all cases, the luminescent materials were exposed to the same level on to the CCD (2400 Digital Numbers) by adjusting the exposure time during image acquisition. The relative exposure periods, shown in the legend, to 2400 DN, and the MTF plots, are shown in Fig. 8.

#### 4.3. Experiment #3, input into a fiber-optic conduit/CCD, the role of the SFO

Experiment #3 was devised to explore the impact of an intermediary SFO or nonscintillating fiber-optic (NSFO) faceplate on phosphor spatial resolution and total light output. Figure 3c provides a summary of the experiment. The SITe 2048 CCD camera that was used in experiment #2, Section 4.2, was used in this experiment. In this series of tests, the Kodak Lanex Fine phosphor was attached to a 7-mm-thick LKH-6 SFO face plate with EMA fibers embedded and to a 5-mm-thick 1.0-NA



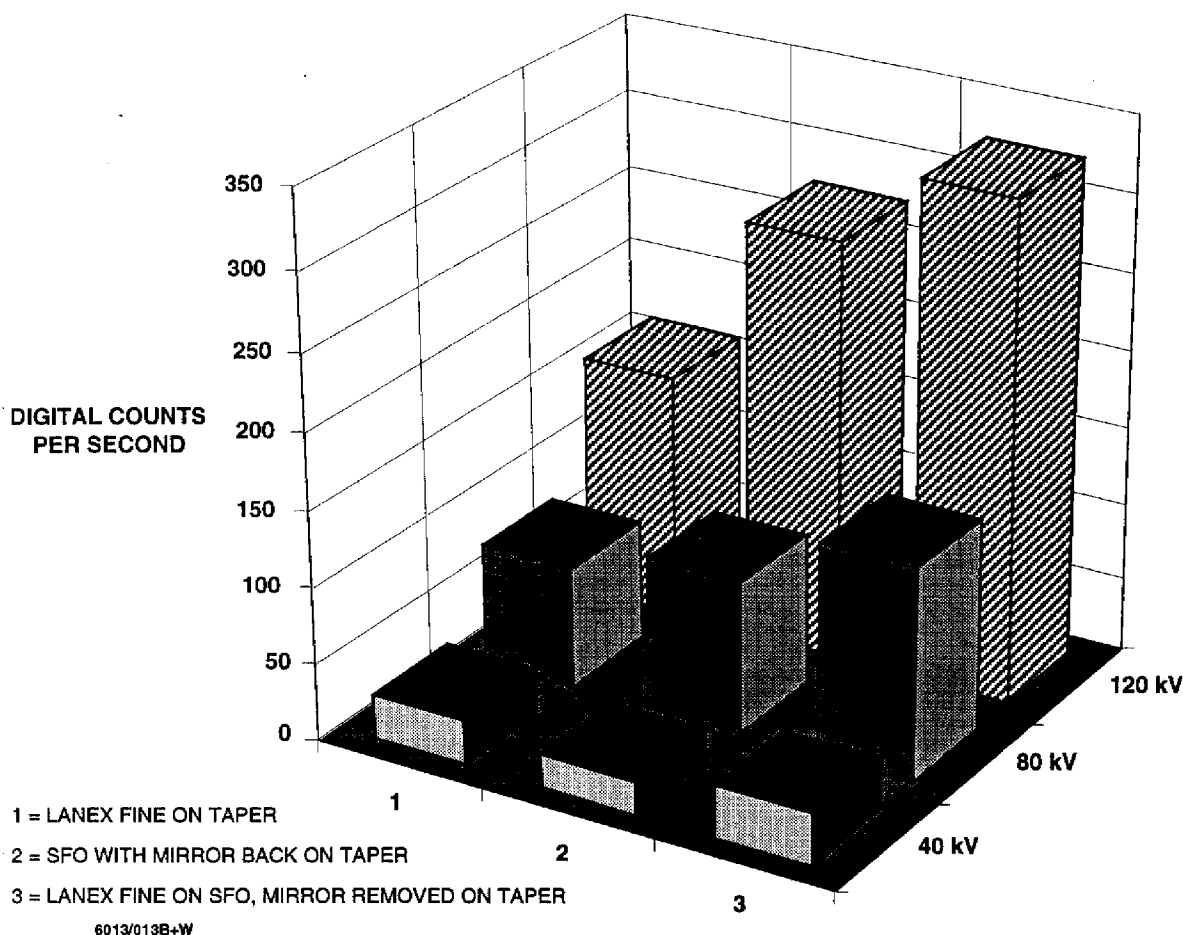


Fig. 7. Brightness values obtained from the MTF measurements acquired in Figs. 4-6.

NSFO and a 0.6-NA NSFO face plate, both without EMA. These combinations were then coupled to the surface of the fiber-optic input conduit. Dow-Corning Q2-3067 coupling grease was used between all interfaces of these three samples.

The highest spatial resolution observable from a lead-filled resolution gauge is reported in Fig. 9. The resolution gauge consists of 0.025 mm of lead, with a bar pattern ranging from 1.5 to 20 lp/mm. The measurements were made at 70 kV. Pixel intensity profiles were used to verify modulation of the highest resolution bar pattern to aid the observer in determining the detectable resolution. Through repeated trials, the highest resolution observable using a line-pair spatial-resolution gage is equivalent to a ~6-8% MTF level using similar x-ray beam conditions. This allows direct quantitative comparison to MTF data in the high-spatial-frequency domain and facilitates comparison of results from experiment #2.

Light measurements were made at 70 kV using a 2-mm Al filter; at 120 kV, using a 19-mm Al and a 1.3-mm Cu filter; and at 160 kV using a 19-mm Al and a 2.9-mm Cu filter using a Philips 160 Industrial x-ray source. The light measurements are reported as relative values to the Lanex Fine/0.6-NA NSFO face plate at each energy. The data is provided in Fig. 9.

## 5. Results

### 5.1. Experiment #1: hybrid scintillators coupled to a CCD through a fiber-optic taper

The first group of tests on the hybrid scintillators developed in this study was performed with a moderate-resolution camera, a system that has a spatial resolution of 10 lp/mm. Since the fiber-optic taper has an effective numerical aperture of only 0.3, the light-acceptance angle from the phosphor samples is no better than approximately  $\pm 17$  deg. Section 4.1 and Fig. 3a provide experimental details. The brightness values for the phosphors studied in this experiment, as a function of x-ray energy, are provided in Fig 7. The MTF results of these materials are shown in Figs. 4-6 for the 40-, 80-, and 120-kV tests respectively. Figure 4 shows that the mirror-backed LKH-6 SFO provides the highest spatial resolution, at 40 kV. It remains

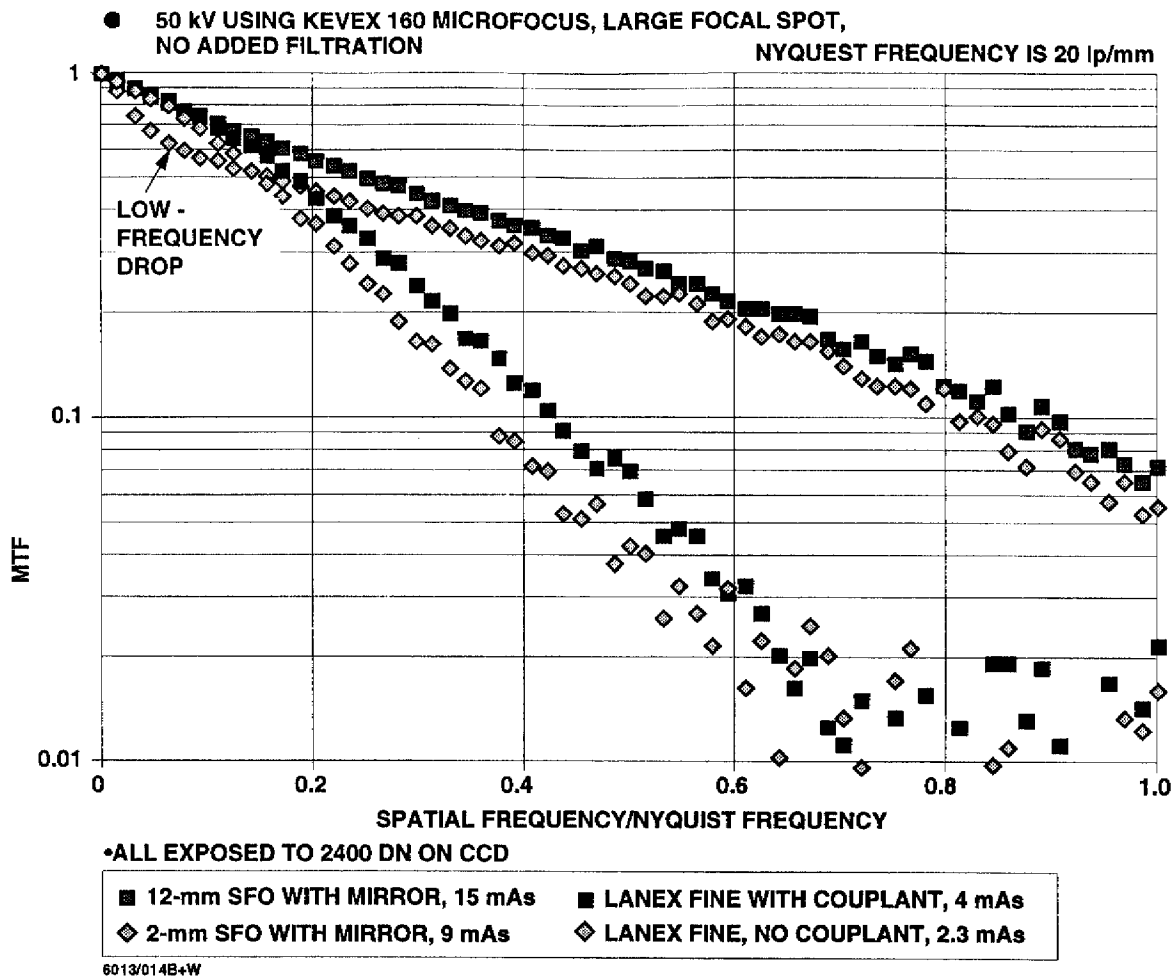


Fig. 8. MTF measurements of SFO plates and Lanex Fine at 50 kV.

highest through the entire spatial frequency spectrum. This same material also has the lowest light output (see Fig. 7). The Lanex Fine phosphor screen is about 1.4 times brighter than the SFO face plate at this energy, but has nearly a factor of 3 lower MTF at the Nyquist frequency of 10 lp/mm. The new hybrid scintillator is the combination of the Lanex Fine and the SFO, as shown schematically in Fig. 1. This hybrid detector provides a modest gain of 14% in light over the Lanex Fine screen alone, without further loss in spatial resolution. This light gain is achieved by absorbing and converting x-ray radiation that has penetrated through the phosphor screen. At 40 kV, the gain due to the SFO is small, since the phosphor is absorbing a large amount of the incident radiation, and the SFO x-ray-to-light conversion efficiency is not as high as that of this phosphor.

As the energy is increased, there are larger light gains from use of the hybrid scintillator, since a large portion of the x-ray fluence is penetrating through the phosphor material that is absorbed by the thicker SFO material. Figure 7 shows that at 80 kV, the hybrid scintillator is 1.75 times brighter than the Lanex Fine material alone, and this increases to 2 times brighter than the Lanex Fine at 120 kV. At 80 kV and 120 kV, there is some minor degradation in the spatial resolution of the hybrid scintillator. In Fig. 6, the hybrid scintillator MTF plot appears to be a combination of the slopes of the two other plots. There is an initial drop-off in the low-frequency MTF region, caused presumably by the parallax effect, as seen in the SFO-only plot. In the mid-MTF range, the hybrid and Lanex Fine plots seem to be nearly parallel, then coalesce to similar levels in the high-spatial-frequency regime. These data indicate that there is some additional glare from the hybrid scintillator in relation to the Lanex Fine, but small features are still discernible, and large gains in light production are achievable through substantial gains in x-ray absorption at these energies. Capturing and converting more x-ray photons in less or equivalent time is critical in improving signal statistics that can lead to improved signal-to-noise levels, reduced quantum mottle, and enhanced feature discrimination.

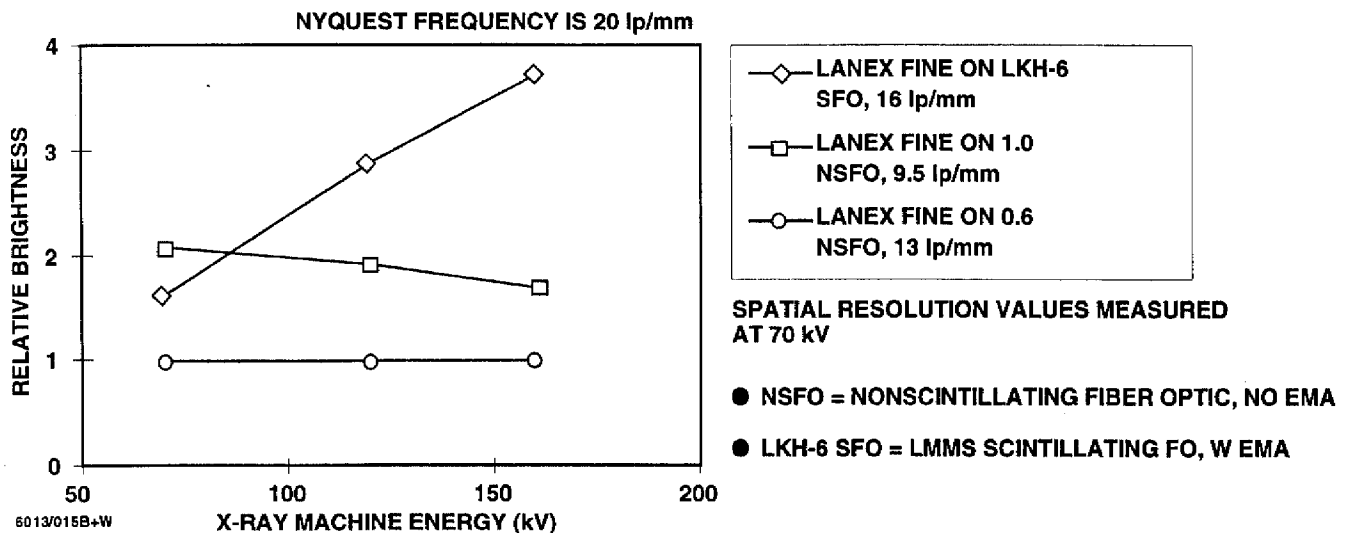


Fig. 9. Relative brightness values as a function of energy for the Lanex Fine phosphor on the LKH-6 SFO and NSFO face plates attached to the conduit. Spatial resolution values are found in the legend.

### 5.2. Experiment #2, the SFO and Lanex Fine separately input onto the conduit of the 20-lp/mm camera

Figure 8 provides MTF plots of a 12-mm-thick mirror-backed SFO, a 2-mm-thick mirror-backed SFO and the Lanex Fine phosphor, all attached directly to the fiber-optic input conduit of the 20-lp/mm camera. The Lanex Fine phosphor was coupled to the conduit with and without coupling fluid, and separate plots are shown for these conditions. Section 4.2 and Fig. 3b provide details of the experiment. The legend in Fig. 8 also provides the exposure levels to reach a common plateau of 2400 DN on the CCD, and therefore provides a measure of comparative screen brightness.

The MTF curves in this figure demonstrate the superior spatial resolution of the SFO luminescent device over the high-resolution phosphor screen. The gap in spatial resolution between the best Lanex plot and best SFO plot in Fig. 8 is much larger than observed with the use of the fiber-optic taper coupled camera discussed in Section 5.1 (Fig. 4). Similarly, the gap in brightness at 40 (50) kV is also much larger in favor of the Lanex Fine phosphor screen over the 12-mm SFO used in both experiments, 1.4 times in experiment #1, 3.75 times in experiment #2. The exit angle of light is greater from the scattered light of the phosphor than from the SFO. Using a high-NA collection device, more high-angle light will be captured than from the taper. Therefore, with the use of the conduit, there is a larger gain in high-angle light from the phosphor in relation to the SFO. This change in collection device reduces the spatial resolution and increases the brightness at the CCD from the phosphor in relation to the SFO alone.

There is a subtle difference between the two SFO plots shown in Fig. 8. There is a low-spatial-frequency drop-off when shifting to a thinner SFO face plate, in this case a 2-mm mirror-backed SFO. In the thinner plate, there are not enough EMA fibers to absorb light that has exceeded the critical angle in the fibers before it is captured by the high-NA-input face plate. Figure 10 illustrates the source of the low-frequency drop-off from thin SFO plates. Coincident with the drop in low-frequency MTF is a reduction in exposure time to reach 2400 DN. This improvement in exposure speed is directly related to the increased stray light being captured by the CCD. In the energy range from 20 to 60 kV, the MTF can be kept high throughout the entire spectrum by use of thicker plates, where EMA stray-light filtration can take effect. Additionally, a higher concentration of EMA fibers can be packed into the face plate to maintain high MTF at low spatial frequencies. Figure 1b shows a photomicrograph of the LKH-6 SFO with EMA fibers every third fiber and every third row

Figure 8 also shows a difference in the spatial resolution and exposure of the Lanex Fine, with and without coupling fluid. Here, as in the thin SFO plate discussion above, the higher brightness levels onto the CCD from the Lanex Fine without coupling fluid come with a diminution in spatial resolution.

### 5.3. Experiment #3. Hybrid scintillators coupled to the 2048 x 2048 CCD camera

With advanced silicon processing methods to develop very large CCD and photodiode sensors, there is an increasing need to develop effective means for coupling the light from phosphor screens directly to the silicon without the use of a lens. As

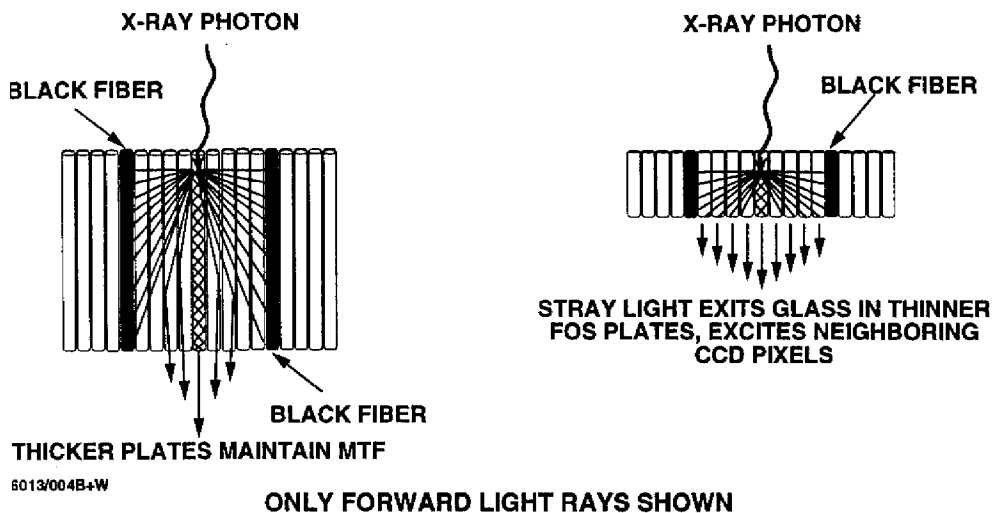


Fig. 10. Role of the SFO thickness on stray-light reduction by the black EMA fibers.

discussed in Section 1, the use of an intermediate fiber-optic transfer conduit is an attractive alternative to lens optics. This section charts the results of intermediary SFO and nonscintillating fiber-optic (NSFO) face plates on phosphor spatial resolution and total light output.

The experimental conditions and samples used in this experiment are described in Section 4.3. Brightness values for the Lanex Fine phosphor screen attached to the LKH-6 SFO, the 0.6-NA NSFO, and the 1.0-NA NSFO, all attached to an input fiber-optic of the CCD, are shown in Fig. 9. Note that the phosphor on the SFO is ~1.7 times brighter than the same phosphor on the 0.6-NA NSFO at 70 kV. This increases to nearly a factor of 4 brighter at 160 kV. This brightness improvement is accompanied by an enhanced spatial resolution of nearly 125% at 70 kV. The added brightness is due to the contribution of light from the SFO, which has a much higher x-ray absorption efficiency than the phosphor screen at these x-ray energies. The resolution values in the legend of Fig. 9 indicate that the SFO is producing a higher resolution image than the phosphor screen, shifting the combined resolution result to higher levels than that of the phosphor light through the 0.6-NA NSFO. It should be noted that the NSFO face plates used in this study have no EMA fibers. An EMA-filled NSFO would provide lower light levels than shown here, although the resolution would be somewhat higher.

The importance of using limited-aperture fiber optics between the phosphor and the CCD can be shown by comparing the results in Fig. 8 with those in Fig. 9. The use of the 0.6-NA NSFO improves the spatial resolution of this phosphor from ~ 9 lp/mm without the added NSFO (see Fig. 8) to 13 lp/mm with the NSFO (see legend in Fig. 9). The larger numerical aperture NSFO (NA = 1.0) captures more stray light from the phosphor, as seen by the increased light levels in Fig. 9 over that of the 0.6-NA NSFO. The high acceptance angle of the 1.0-NA NSFO results in a spatial resolution measurement of 9.5 lp/mm, which is similar to that made without an added fiber optic (Fig. 8).

As in the studies performed using a taper input face plate, at 160 kV, Figs. 4 through 6, the low-frequency spatial resolution of the hybrid scintillator drops off with increasing energy, but the high-frequency MTF stays much higher than that of the phosphor-coupled NSFO face plates. Therefore, high x-ray absorption, high brightness (levels as high as 4 times greater), and very high image detail can be obtained by using hybrid scintillators as compared to using phosphors alone or with nonscintillating fiber-optic face plates.

## 6. Discussion

The hybrid scintillators combine light from a phosphor screen or layer with light from a scintillating fiber-optic under x-ray illumination. The SFO, since it is formed of light-guiding fiberglass, can be made thicker than phosphor screens. The thicker SFO can absorb a much larger portion of the x-ray imaging photons than the phosphor screens can (see Fig. 10). Furthermore, since the SFO has a small fiber size, with a limited numerical aperture, the light produced is directed to a sharp image plane at the surface of the face plate, resulting in high-spatial-resolution imagery. Phosphor screens produce light throughout the screen thickness without collimation. Light produced anywhere in the thickness of the screen will scatter and spread prior to capture by the next element in the imaging chain. By using a limited-aperture collector, such as an LMMS-designed SFO, some of this

stray light will either not enter the SFO or be absorbed in the EMA of the SFO prior to being collected by a light sensor array. An attractive aspect of using phosphor screens is that they are more efficient than the SFO in converting absorbed x-ray photons to light. By accepting a lower angle of emitted light from the phosphor, in combination with the trapped SFO light, the hybrid scintillator produces higher spatial resolution than can be obtained from a phosphor alone, and higher brightness values than can be achieved from the SFO or phosphor alone.

Phosphor materials are sometimes selected based on the wavelength sensitivity of the sensor used in the light-collection device. Tube-based photocathode detectors and silver halide-based films are more effective capturing blue-green light. CCD and silicon photodiode arrays have a high quantum efficiency in the green-to-red spectral range. X-ray phosphor materials available range from high Z and high brightness to moderate Z and low brightness to meet specific spectral characteristics. The use of the SFO in the hybrid scintillator is less important at low x-ray energies (i.e., in the 10-30 kV range) with high-Z, high-brightness phosphor materials. With selection of moderate-Z, moderate-brightness phosphor materials, the SFO can play a greater role in total brightness at lower x-ray energies resulting in needed light gain while maintaining or improving spatial resolution. With all phosphors, as the x-ray energy is increased, the SFO begins to absorb a greater and greater portion of the x-ray photons over the phosphor, and begins to exceed the light gain of the phosphor in the combined device. With the increase in energy, however, there is a drop in the low-frequency MTF with the use of the thicker sensors. This usually does not effect the high-spatial-frequency domain and high-detail features are still distinguishable in the x-ray pictures acquired.

The improvement in light output gained by using the hybrid scintillator instead of the phosphor material depends on the numerical aperture of the input device to the electronic sensor. A high-NA collection device captures more stray light from a phosphor than from a hybrid scintillator or an SFO. This results in a smaller improvement in brightness from the hybrid scintillator than is observed with lower NA optics. However, the improvement in spatial resolution obtained by the SFO hybrid scintillator detector is greater with the use of the high-NA optics.

## 7. Conclusions

Hybrid scintillators have been shown to improve the x-ray absorption, enhance light levels, and maintain or improve the spatial resolution of phosphor materials. These gains are obtained without the development of new phosphor materials. The LKH-6 SFO has been shown to be a good candidate for combination with x-ray phosphor materials to result in improved x-ray imaging properties. The hybrid scintillator can be configured to meet specific spatial-resolution and output requirements in different light-based x-ray imaging systems.

Studies of these hybrid scintillators are continuing with different phosphor materials of various packing densities using different optical setups and cameras.

## 8. Acknowledgments

The authors are grateful to Professor Thomas J. Beck at the Johns Hopkins University, Department of Radiology, for helpful discussions on methods to enhance the brightness of scintillators. The authors also wish to thank Mr. H. John Ellis and Mr. Richard W. Mead of Collimated Holes, Inc., for helpful discussions and for providing samples of fiber-optic imaging face plates.

## 9. Appendix

In general, the spatial resolution of an imager may be characterized by the full width at half maximum (FWHM) of its point-spread function (PSF). The PSF could be measured by imaging a pinhole which is smaller than one pixel in diameter. An alternative is to express horizontal resolution using the line-spread function (LSF) of a vertical line, and similarly the vertical resolution using the LSF of a horizontal line. For a square CCD (in a symmetrical system) the resolution should be the same in either direction. We use the LSF because a vertical line will cross many rows of pixels, yielding many measurements on a single exposure, which can then be averaged for a result less subject to statistical noise. In practice, the LSF can be measured directly by imaging a thin (less than 1 pixel) high-contrast wire, or the inverse, imaging a similarly narrow slit. Barrett and Swindell,<sup>10</sup> for example, detail the relationship between such a one-dimensional delta function x-ray input and an imager's MTF. A mechanical design for a variable-width slit suitable for x-rays, and some resulting measurements, are presented by Roehrig et al.<sup>11</sup>

A more manageable experimental setup is the imaging of a simple straightedge. The pixel intensity profile across a sharp edge (step function in density) is the edge response function (ERF), the derivative of which is the related LSF. An explicit presentation of the mathematics, assuming a Gaussian LSF, is given by Bentzen.<sup>12</sup> The Fourier transform of the LSF is the modulation transfer function (MTF), a function of spatial frequency. Our radiograph spatial resolution evaluations are displayed as semilogarithmic plots of the normalized MTF as a function of spatial frequency from zero ("dc") to the Nyquist frequency (inverse of 2-pixel width).

The precise alignment of the straightedge with respect to the CCD pixel array is a potential source of an aliasing effect on the LSF. An edge aligned with a column of pixel centers will produce a result different from that of an edge aligned along the boundary between pixel columns. This digital pitfall is elucidated by Fujita et al.,<sup>13</sup> and they develop a method of avoiding the consequences by slightly tilting their slit with respect to the CCD array alignment and thus "finely sample" the LSF. The distance between slit center and pixel center differs slightly from row to row in a fashion straightforwardly calculable from the tilt slope, allowing the LSF to be characterized with an effectively sub-pixel resolution.

In our measurements we tilt a tungsten straightedge by 5 to 10 deg to accomplish this fine sampling of the edge response function. After dark current subtraction and image flat-fielding correction, a small program written in C++ finds the edge, determines its slope, and builds an ERF. The ERF is differentiated to obtain an LSF, and then fast Fourier transformed to derive the MTF, which is written to a file. Display plots are generated with Microsoft Excel. These results are found to be reproducible independent of the exact straightedge angle orientation.

## 10. References

1. H. J. Ellis, Collimated Holes, Inc., Campbell, CA, unpublished methods.
2. C. Bueno and R. A. Buchanan, "Terbium Activated Silicate Luminescent Glasses for Use in Converting X-Ray Radiation into Visible Radiation," US Patent 5,122,671, June 16, 1992; C. Bueno and R. A. Buchanan, "Terbium Activated Silicate Luminescent Glasses," U. S. Patent 5,391,320, February 21, 1995.
3. G. Y. Fan, C. Bueno, D. Dunkelberger, and M. H. Ellisman, "Performance characteristics of radioluminescent fiber optics as electron scintillators," *J. Electron Microscop.*, Vol. 42, pp. 419-423, 1993.
4. R. C. Placious, D. Polansky, H. Berger, C. Bueno, C. L. Vosberg, R. A. Betz, and D. J. Rogerson, "A high density glass scintillator for real-time x-ray inspection," *Materials Evaluation*, Vol. 49 (11), pp. 1419-1421, 1991.
5. C. Bueno and R. A. Buchanan, "Luminescent glass design for high energy realtime radiography," in *Properties and Characteristics of Optical Glass II, Proc. SPIE*, Vol. 1327, pp. 79-91, 1990.
6. C. Bueno and M. D. Barker, "High resolution digital radiography and three-dimensional computed tomography," in *X-ray Detector Physics and Applications II, Proc. SPIE*, Vol. 2009, pp. 179-191, 1993.
7. C. Bueno and M. D. Barker, "High resolution digital radiography and three dimensional computed tomography of composite materials," *Proceedings of the 39th International SAMPE Symposium and Exhibition*, April 11-14, 1994, pp. 766-778, 1994.
8. C. Bueno, M. D. Barker, P. E. Condon, and R. A. Betz "Solid state x-ray imaging methodology," *Final Report, WL-TR-92-4003*, March, 1992.
9. C. Bueno, M. D. Barker, R. A. Betz, R. C. Barry, and R. A. Buchanan, "Nondestructive evaluation of aircraft structures using high resolution real-time radiography," in *Nondestructive Evaluation of Aging Aircraft, Airports, Aerospace Hardware, and Materials*, Tobey M. Cordell, Raymond D. Rempt, Editors, Proc. SPIE, Vol. 2455, pp. 114-124, 1995.
10. Barrett, H. H., and W. Swindell, *Radiological imaging: the theory of image formation, detection, and processing*, Vols. 1 and 2, Academic Press, New York, 1981.
11. Roehrig, H., T-Y. Fu, and D. Yocky, "X-ray slit for the measurement of the MTF of x-ray image intensifiers from the linespread function," *Interim Report Grant 5 ROI-FD-00804*, Dept. of Radiology, Arizona Health Sciences Center, University of Arizona, Tucson, March 1985.
12. Bentzen, S. M., "Evaluation of the spatial resolution of a CT scanner by direct analysis of the edge response function," *Medical Physics*, Vol. 10, p. 579, 1983.
13. Fujita, H., D-Y. Tsai, T. Itoh, K. Doi, J. Morishita, K. Ueda, and A. Ohtsuka, "A simple method for determining the modulation transfer function in digital radiography," *IEEE Transaction on Medical Imaging*, Vol. 11, pp. 34-39, 1992.